RESEARCH

Fourier transform infrared spectral features of plant biomass components during cotton organ development and their biological implications

HE Zhongqi[1]* , LIU Yongliang[1], KIM Hee Jin[1], TEWOLDE Haile[2] and ZHANG Hailin[3]

Abstract

Background: The majority of attenuated total reflection Fourier transform infrared (ATR FT-IR) investigations of cotton are focused on the fiber tissue for biological mechanisms and understanding of fiber development and maturity, but rarely on other cotton biomass components. This work examined in detail the ATR FT-IR spectral features of various cotton tissues/organs at reproductive and maturation stages, analyzed and discussed their biological implications.

Results: The ATR FT-IR spectra of these tissues/organs were analyzed and compared with the focus on the lower wavenumber fingerprinting range. Six outstanding FT-IR bands at 1 730, 1 620, 1 525, 1 235, 1 050 and 895 cm^{-1} represented the major C=O stretching, protein Amide I, Amide II, the O–H/N–H deformation, the total C–O–C stretching and the β-glycosidic linkage in celluloses, respectively, and impacted differently between these organs with the two growth stages. Furthermore, the band intensity at 1 620, 1 525, 1 235, and 1 050 cm^{-1} were exclusively and significantly correlated to the levels of protein (Amide I bond), protein (Amide II bond), cellulose, and hemicellulose, respectively, whereas the band at 1 730 cm^{-1} was negatively correlated with ash content.

Conclusions: The resulting observations indicated the capability of ATR FT-IR spectroscopy for monitoring changes, transportation, and accumulation of the major chemical components in these tissues over the cotton growth period. In other words, this spectral technology could be an effective tool for physiological, biochemical, and morphological research related to cotton biology and development.

Keywords: Cotton, Fourier transform infrared spectroscopy, Fiber, Cellulose, Protein, Plant tissue

Introduction

Cotton (*Gossypium* spp) is grown in over 100 countries/regions covering an area of 33 million hectare and is fulfilling around 31% of fiber needs for textile purposes (Mollaee et al. 2020). It also produces edible oil from cottonseed for human consumption, and cottonseed meal as animal feed (Cheng et al. 2020; Kumar et al. 2021).

Other cotton organs or biomass byproducts could also be used as animal feed supplements, bioenergy sources, soil amendments, and industrial raw materials (Al Afif et al. 2020; He et al. 2016, 2020b; Kirkan et al. 2018; Kurtulbaş et al. 2018; Vancov et al. 2018; Yue et al. 2020). Furthermore, biological importance of different tissues of cotton plants (e.g., leaves, bolls, stalks, and stems), components of cotton leaves and their functional role/biological activities, and effect of cotton leaf traits (e.g., leaf color phenotypes and curly leaf morphology) on cottonseed nutritional qualities have been investigated (Bellaloui et al. 2019, 2021; Egbuta et al. 2017; Shakhidoyatov et al.

*Correspondence: zhongqi.he@usda.gov
[1] Southern Regional Research Center, USDA-ARS, New Orleans, LA 70124, USA
Full list of author information is available at the end of the article

HE *et al. Journal of Cotton Research*   (2022) 5:11

Page 2 of 13

1997). However, their correlation with Fourier transform infrared (FT-IR) features have not been well characterized (He and Liu 2021). FT-IR spectroscopy has been widely used to characterize various agricultural biomass materials (Bekiaris et al. 2020; Goydaragh et al. 2021; He et al. 2009, 2011; Hssaini et al. 2021; Lazzari et al. 2018; Waldrip et al. 2014). Especially, combined with attenuated total reflection (ATR) sampling device, FT-IR method has facilitated the research of different cotton plant related materials (Cheng et al. 2019; He et al. 2021a; Kim et al. 2017; Nam et al. 2017). However, the majority of the FT-IR investigations are focused on the fiber tissue for biological mechanisms and understanding of fiber development and maturity, but rarely on other cotton biomass components and their biological implications (Abidi et al. 2014; He and Liu 2021; Liyanage and Abidi 2019; Natalio and Maria 2018). One representative study was to monitor changes in cellulose within developing cotton fibers at 10 to 56 days postanthesis (DPA) between two cultivars (TM-1 and TX55) by Abidi et al. (2014). Their results revealed the usefulness of the integrated intensities of the bands at 3 286, 1 738, 1 639, 1 543, 1 161, 897, 710, and 667 cm^{-1} in evaluating the secondary cell wall cellulose formation, especially, the potential of the integrated intensities of two bands at 897 and 667 cm^{-1} in assessing cotton fiber cellulose content indirectly. For the same two cultivars, Abidi and Manike (2018) reported the linear response of the percentage crystallinity from wide-angel X-ray diffraction to either the two-band ratio at 1 372 and 2 900 cm^{-1} or the single-band integrated intensities of two bands at 667 or 897 cm^{-1}. In order to evaluate cotton fiber development directly and quantitatively, Liu and Kim (2017) and Liu et al. (2011) identified a number of unique IR bands, and then proposed simple algorithms for fiber maturity with the use of three IR band intensities at 1 500, 1 032, and 956 cm^{-1}, for fiber crystallinity with the use of three IR band intensities at 800, 730, and 708 cm^{-1}, and also for developmental index with the use of three IR band intensities at 1 800, 1 315, and 1 236 cm^{-1}. In addition, there are a few studies on FT-IR features of cotton plant materials (e.g., leaf, hull, stem, bract, and seed coat) (Allen et al. 2007; Fortier et al. 2011, 2017; Himmelsbach et al. 2006). These FT-IR studies of cotton plant derivatives are mainly for their identification and detection due to their presence as contaminants mingled into commercial cotton fiber, not for biological characterization of these biomass fractions during different growth phases.

In exploring and optimizing crop management practices, He et al. (2017, 2020a) collected different cotton plant biomass fractions from field-grown cotton plants at the reproductive stage (i.e., mid-season) and the maturation stage (i.e., late season just before defoliation for

harvesting readiness), and reported their elemental composition and biomolecule (e.g., carbohydrate and amino acid) profiles. In the meantime, the ATR FT-IR spectra of these biomass samples were also briefly examined, demonstrating the potential of ATR FT-IR as a diagnostic tool for monitoring plant biomass biosynthesis for cotton physiology and biology research (Liu et al. 2016). It is also reported that the FT-IR data of different stem parts of *Arabidopsis thaliana* have been applied for metabolic fingerprinting of the wild type and mutant lines (Brown et al. 2005). Thus, in this work, we examined in detail the ATR FT-IR spectral features of these biomass samples, analyzed and discussed their biological implications. As ATR FT-IR spectroscopy could identify exclusively and consistently the major chemical components (e.g., protein, hemicellulose) in different cotton tissue materials, it was hypothesized that such a capability would make this spectral technology an effective monitoring tool for physiological, biochemical, and morphological research related to cotton biology and development (Brown et al. 2005). Our overall goal is to provide more knowledge about cotton biology and development for researchers and growers to optimize field management practices and processing strategies for higher yield and quality of cotton fiber and biomass materials as valuable natural resources.

Materials and methods

Cotton materials and sample preparation

Two sets of cotton plant biomass materials were collected and used in the work. The details of collection and treatment of the first set of samples were reported previously (He et al. 2017, 2020a). Briefly, they were prepared from a cotton variety Deltapine (DP) 1321 B2RF grown at the Mississippi Agricultural and Forest Experiment Station near Pontotoc, MS (34° 8′ 30″ N, 88° 59′ 36″ W) (Tewolde et al. 2015). The soil type was Atwood silt loam. Four to eight whole plants from each plot of four replications were collected in 80 and 112 days after planting (DAP) that were classified into vegetative, reproductive, and maturation stages, respectively (Fig. 1). The cotton plants in the reproductive stage were separated into six different organs including main stem, branch stem, leaf blade, petioles, root, and reproductive tissues (Figs. 1B, 2A). In addition to the six organs, fiber and seeds were also classified from the cotton plants in the maturation stage (Figs. 1C, 2B). The seed samples were delinted with concentrated H_2SO_4, rinsed with tap water, and dried in a forced-air oven at 80 °C (He et al. 2020c). All samples except for cotton fibers were ground to < 1 mm and kept at a relative humidity of $(65 \pm 2)\%$ and temperature of (21 ± 2) °C prior to characterization. Cotton fibers

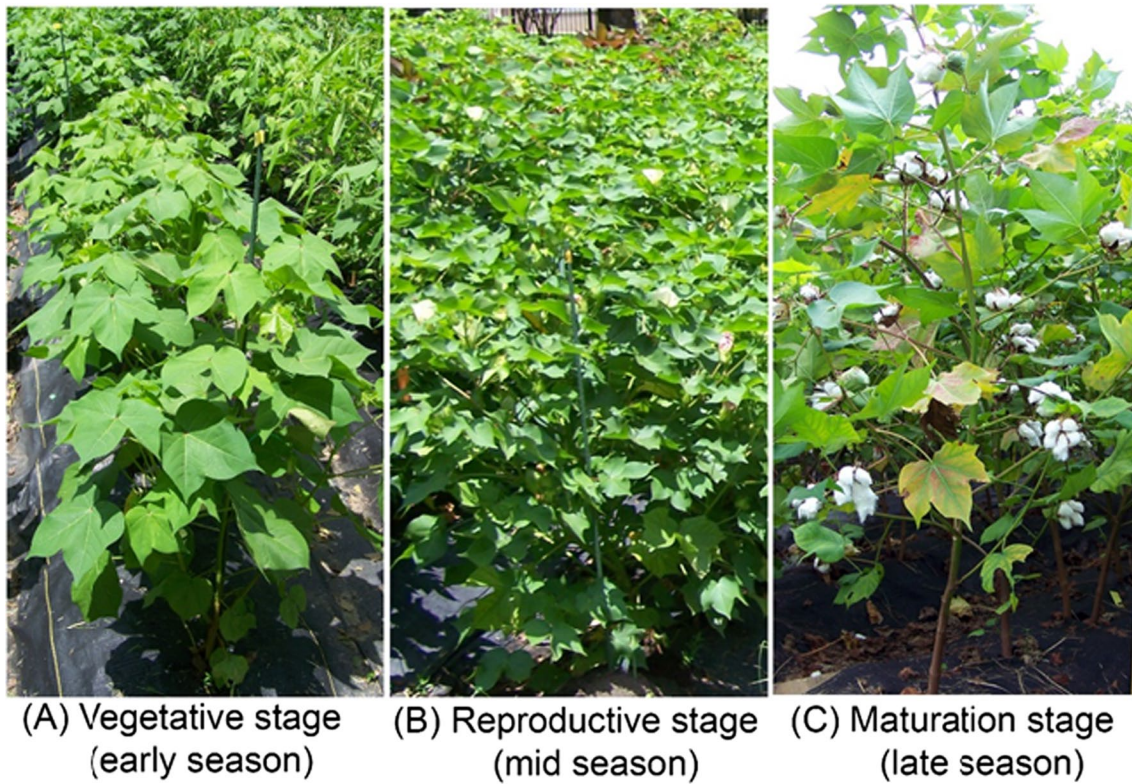HE *et al. Journal of Cotton Research*   *(2022) 5:11*

Page 3 of 13

Fig. 1 Seasonal development of cotton. Cotton developmental stages were classified according to the three different seasons described in Oosterhuis and Jernstedt (1999). Green garden stakes (90 cm) were used as a scale marker
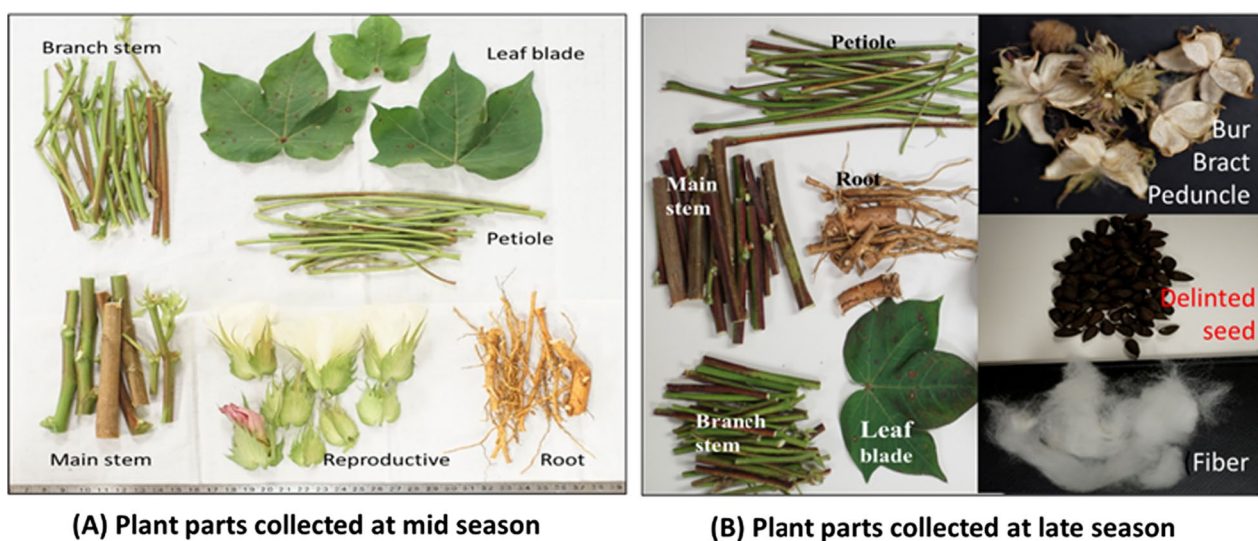

Fig. 2 Cotton plant biomass fractions used in this study. **A** and **B** collection of plant organs of variety DP 1321 B2RF, at reproductive stage (mid-season) and maturation stage (late season at pre-defoliation for harvesting), respectively. Bur, bract, and peduncle are not separated

separated from the seeds were subjected to the FT-IR analysis without further treatment.

ATR FT-IR spectral collection and analysis

All samples were conditioned at a constant relative humidity of (65 ± 2)% and temperature of (21 ± 2) °C for at least 24 h, prior to ATR FT-IR spectral acquisition. An FTS 3000MX FT-IR spectrometer (Varian Instruments, Randolph, MA, USA), aligned with ATR attachment, was employed to collect ATR FT-IR spectra. It was equipped with a ceramic source, KBr beam splitter, and deuterated triglycine sulfate (DTGS) detector (Liu et al. 2015, 2016; Liu and Kim 2017). The ATR sampling device utilized a DuraSamplIR single-pass diamond-coated internal reflection accessory (Smiths Detection, Danbury, CT, USA), and a consistent contact pressure was applied by way of a stainless steel rod and an electronic load display. Least three measurements for individual sample were collected over the range of 4 000–600 cm^{-1} at 4 cm^{-1} and 16 co-added scans. The spectra were present in absorbance and no ATR correction was applied. Spectral normalization was performed based on the mean of peak intensities from the 1 800–600 cm^{-1}. The mean intensities (i.e., band heights) of interesting bands centered at 1 730, 1 620, 1 525, 1 235, 1 050, and 895 cm^{-1} were determined by a multi-point average of the intensities at respective range of 1 760–1 700, 1 700–1 570, 1 570–1 480, 1 290–1 200, 1 200–910, and 910–880 cm^{-1}.

Chemical composition measurements

Moisture content was determined as the loss in weight upon drying a sample in a forced draft oven at 105 °C for 5 h (McCall and Jurgens 1951). All the measured data in this section were converted to a dry basis via the correction of the moisture content. Ash content was determined by measuring the residual mass of a sample (1.0 g) after heating in a muffle furnace at 550 °C for 4 h. Selected mineral contents were analyzed following acidic digestion. Specifically, 0.50 g of ground sample was mixed in 10.0 mL of concentrated trace metal grade HNO$_3$ for 1 h in a HotBlock™ Environmental Express Block Digester. The sample was then heated to 115 °C for 2 h and 15 min. The concentrations of six macro elements (i.e. P, Ca, K, Mg, Na, and S) and seven trace elements (i.e. Fe, Zn, Cu, Mn, B, Ni, and Al) in these digests were determined by a Spectro CirOs ICP Spectrometer (Mahwah, NJ, USA).

Content of cellulose was calculated by the difference between acid detergent fiber (ADF) and acid detergent lignin (ADL). Hemicellulose content was determined by the difference between neutral detergent fiber (NDF) and ADF. The values of ADF, NDF, and ADL were determined using the filter bag methods with a Fiber Analyzer

(Ankom Technology, Macedon, NY, USA). The total N and C contents of the ground samples were directly determined by a LECO Truspec Dry Combustion C/N Analyzer (St. Joseph, MI, USA) without pretreatments. Crude protein content was calculated by multiplying the N content value by the factor of 6.25 (He et al. 2014).

Data treatment and statistical analysis

The averaged FT-IR spectra of the same type of biomass fractions were reported previously (Liu et al. 2016). However, those data were analyzed as groups without elaboration of their detailed features. In this work, ATR FT-IR spectral features of each sample were re-analyzed with quantitative data of band height. Furthermore, the correlation analyses were performed. The data of contents of selected elements, carbohydrate, and amino acids of various cotton organs collected from the Mississippi field were reported in He et al. (2017, 2020a). In this work, these data were used to calculate the correlation coefficients between the chemical properties and the FT-IR band features. These coefficient values were then discussed to explore the biological implications of these FT-IR features.

The quantitative spectral data (band height) were loaded into Microsoft Excel 2016 to execute simple algorithmic analysis. Separately, *P* values were calculated using one-way analysis of variance (ANOVA) under Data Analysis in Microsoft Excel 2016. The Descriptive Statistics Tool Data were used to calculate means and standard errors of tetraplicate field samples. The Correlation Analysis Tool was used to analyze correlation coefficients between the data sets of different parameters.

Results and discussion

Classification of cotton tissues and organs at two different developmental stages

Fig. 1 shows three different developmental seasons of a cotton variety DP 1321 B2RF used in this study. In the early season (Fig. 1A), vegetative development occurred for establishing roots and expanding leaf area (Oosterhuis and Jernstedt 1999; Robertson and Roberts 2010). In the mid-season (Fig. 1B), reproductive growth began with the emergences of floral buds or squares around 40 DAP. Flowers and developing bolls appeared during the reproductive stage (Fig. 1B). In the late season (Fig. 1C), mature cotton bolls started to open approximately at 100 DAP, and fibers were exposed to air.

The first set of cotton plants was collected in 80 DAP that was in the midst of the reproductive stage (Fig. 1B). They were classified into 6 different organs as shown in Fig. 2A. Unlike the five different vegetative organs (main stems, branch stems, leaf blades, petioles, and roots), the reproductive tissues were composed of multiple organs

HE *et al. Journal of Cotton Research*   (2022) 5:11

Page 5 of 13

including squares, flowers (yellowish petals, 0 DPA), and young bolls (reddish petals, < 3 DPA) with bracts and peduncles as shown in Fig. 2A. The cotton ovules inside the young cotton bolls contained fiber initials composed exclusively of the primary cell walls since the secondary cell walls were produced after 23 DPA (Abidi et al. 2014; Kim 2015).
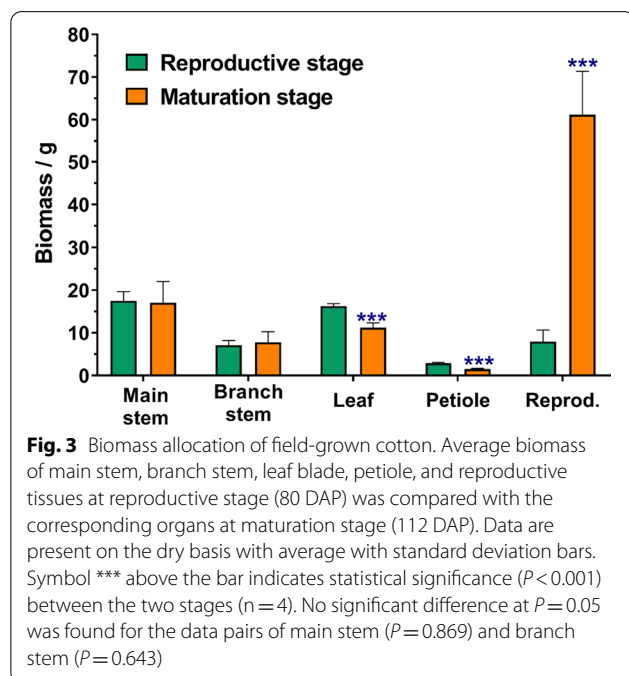
The second set of cotton plants was harvested in 112 DAP that was at the maturation stage of the late season before defoliation for harvesting readiness (Fig. 1C). In addition to the five vegetative organs (main stems, branch stems, leaf blades, petioles, and roots), the mature cotton bolls were separated into three types including seeds, fibers, and others (burs, bracts, and peduncles) as shown in Fig. 2B. Fully developed fibers are composed of almost pure cellulose (Kim 2015).

On the dry basis, the average biomass of main stem at the maturation stage (17.1 ± 5.0 g) shows no significant difference ($P = 0.869$) with that at the reproductive stage (17.5 ± 2.1 g) as shown in Fig. 3. Similarly, the biomass of branch stem also shows no significant variation ($P = 0.643$) between the reproductive (7.1 ± 1.1 g) and maturation (7.8 ± 2.5 g) stages. The similar biomass patterns of both stems between the two stages are expected based on the almost identical cotton heights between the reproductive (89.1 ± 5.9 cm) and maturation (90.3 ± 14.6 cm) stages. In contrast, the average biomass of leaf blades (11.2 ± 1.1 g) and petioles (1.5 ± 0.2 g) at the maturation stage are significantly ($P < 0.001$) reduced compared with the leaf blades (16.3 ± 0.6 g) and petioles

(2.9 ± 0.2 g) at the reproductive stage (Fig. 3). These patterns are consistent with the leaf wilting and abscission process at the maturation stage as shown in Fig. 1C. The average biomass of the reproductive organs strikingly and significantly ($P < 0.001$) increases at the transition from the reproductive stage (8.0 ± 2.7 g) to the maturation stage (61.2 ± 10.3 g) because of the seed and fiber development. We excluded cotton root biomass comparison in Fig. 3 due to practical difficulties of digging up entire cotton roots of individual plants. Under regular field conditions, cotton roots can grow three times more than the aboveground portion of the cotton plant (Oosterhuis and Jernstedt 1999).

ATR FT-IR features of six biomass samples collected at the reproductive stage

Fig. 4 shows the representative ATR FT-IR spectra in the 3 800–600 cm^{-1} region of six different cotton biomass samples collected from the reproductive stage (or mid-season). Although these cotton plant fractions are inherently different, their FT-IR spectra in Fig. 4 are quite similar. This is due to the fact that these natural materials areprimarily composed of varying types of carbohydrates in the forms of cellulose, hemicellulose, pectins, lignins, and sugars, and also of small amounts of proteins, waxes, and other inorganics. FT-IR spectral features of these cotton crop related components, if not all, have been investigated in detail for a variety of interests, and characteristic bands have been assigned to different functional groups (Himmelsbach et al. 2003, 2006; Liu et al. 2012). Typically, the broad and strong bands from 3 700 to 3 000 cm^{-1} region are due to the O–H or N–H stretching modes of carbohydrates, adsorbed water, and proteins, while relatively weak bands at 2 924 and 2 850 cm^{-1} are owing to hydrophobic CH$_2$ asymmetrical and symmetrical stretching vibrations, respectively (He et al. 2021b; Zhang et al. 2021). One band close to 1 730 cm^{-1} contributed by the C=O stretching modes of carbonyl groups (Himmelsbach et al. 2003) should be due to the minor organic acids (e.g., malic and citric acid) (He et al. 2009; Wakelyn et al. 2007). The broad band centered at 1 620 cm^{-1} and the minor band at 1 520 cm^{-1} are mainly from the O–H bending, Amide I and II (N–C=O) of protein and pectic acid esters as well as H-bonded C=O of conjugated ketones (Abidi et al. 2014; He et al. 2009). Numerous absorptions in the region of 1 500–1 200 cm^{-1} consist of a combination of CH$_2$ deformations and C–O–H bending vibrations, and those in the 1 200–800 cm^{-1} region are ascribed to the C–O and C–C stretching vibrations. Especially, the outstanding band around 1 020 cm^{-1} is mainly due to C–O stretching of carbohydrates in these plant materials although some inorganic components (e.g., P–O, Si–O bonds) may also

Fig. 3 Biomass allocation of field-grown cotton. Average biomass of main stem, branch stem, leaf blade, petiole, and reproductive tissues at reproductive stage (80 DAP) was compared with the corresponding organs at maturation stage (112 DAP). Data are present on the dry basis with average with standard deviation bars. Symbol *** above the bar indicates statistical significance ($P < 0.001$) between the two stages (n = 4). No significant difference at $P = 0.05$ was found for the data pairs of main stem ($P = 0.869$) and branch stem ($P = 0.643$)

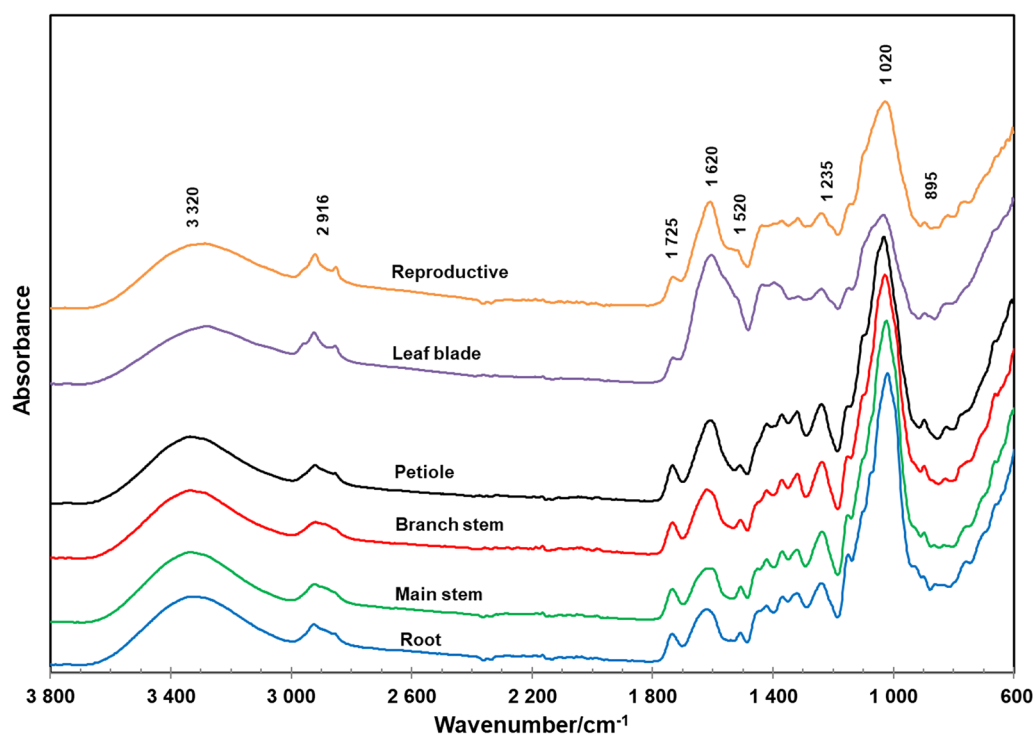HE *et al. Journal of Cotton Research*   (2022) 5:11

Page 6 of 13

Fig. 4 ATR FT-IR spectra of six different cotton organs and tissues collected from cotton plants at the reproductive stage

have some contribution (Bekiaris et al. 2015; He et al. 2006; Himmelsbach et al. 2006). A weak absorption near 895 cm^{-1} is attributable to β-glycosidic linkage in linear cellulose portion of cotton fibers, as its integrated intensity or area was proportional positively to the percentage of cotton cellulose content (Abidi et al. 2014; Bekiaris et al. 2015; Liu and Kim 2017).

Chemically, stem-like substances, represented by root, main stems, and branch stem, are mainly composed of carbohydrates at varying amounts and derivatives, such as cellulose, hemicellulose, pectins and lignins, and also other organic/inorganic components (Renuka et al. 2005). Whereas leaf-like samples, such as petioles, leaf blade, and reproductive tissues, are comprised of hydrocarbons, organic/amino acids, phenolic compounds, carotenoids, sugars, pectins, and others (Shakhidoyatov et al. 1997). Visually, these cotton plant biomasses exhibit similar FT-IR features, but with differences in relative band intensities and positions. For example, the intensity of the band around 1 620 cm^{-1} increased from the root material, along with the biomass order of the plant topology, to the reproductive material. Thus, it was estimated that this band and other bands in the lower wavenumber range (i.e., the fingerprinting region) may be applicable, while the two band groups (i.e., around 3 320 cm^{-1} covering the 3 700–3 000 cm^{-1} and 2 900 cm^{-1} covering the 3 000–2 800 cm^{-1}) in the high wavenumber wing

are too broad or weak for meaningfully quantitative applications. To this regard, the fingerprinting region was divided into six spectral intervals subjectively, with the 1 760–1 700 cm^{-1} region noted as $I_{1\ 730}$ representing C=O stretching modes typically from esters, ketones, and acids, the 1 700–1 570 cm^{-1} region noted as $I_{1\ 620}$ presenting the overlapped contributions from adsorbed water at 1 640 cm^{-1} and proteins (Amide I) at 1 620 cm^{-1}, the 1 570–1 480 cm^{-1} region noted as $I_{1\ 525}$ originating from proteins (Amide II), the 1 290–1 200 cm^{-1} region noted as $I_{1\ 235}$ focusing on O–H or N–H deformation, the 1 200–910 cm^{-1} region noted as $I_{1\ 050}$ showing a total C–O–C stretching contributed from all C–O–C containing substances regardless of cellulosic or non-cellulosic molecules, and the 910–880 cm^{-1} region noted as I_{895} considering the sole origin of β-glycosidic linkage in cellulose (Table 1). It is worth noting that the subjective division of the fingerprinting region into six spectral intervals is more complicated than those relevant studies which focused more on fewer band regions for fiber quality, maturity and crystallinity indices (He and Liu 2021).

As given in Table 1 from the reproductive stage, the intensities of three bands at 1 620 cm^{-1} ($I_{1\ 620}$), 1 525 cm^{-1} ($I_{1\ 525}$), and 1 235 cm^{-1} ($I_{1\ 235}$) increase from root material to main stem, branch stem, petiole, and leaf blade, but the reproductive specimen has reduced intensities compared with the leaf blade sample. The intensities

HE *et al. Journal of Cotton Research* (2022) 5:11

Page 7 of 13

Table 1 The normalized intensities of six ATR FT-IR bands of the plant biomass from the reproductive stage. Data are presented as average ± standard deviation (n = 4)

	$I_{1\,730}$	$I_{1\,620}$	$I_{1\,525}$	$I_{1\,235}$	$I_{1\,050}$	I_{895}
Reproductive	0.36 ± 0.00	0.79 ± 0.02	0.62 ± 0.02	0.89 ± 0.01	1.36 ± 0.02	0.90 ± 0.01
Leaf blade	0.34 ± 0.00	1.00 ± 0.02	0.91 ± 0.02	0.92 ± 0.01	1.17 ± 0.02	0.76 ± 0.01
Petiole	0.41 ± 0.01	0.67 ± 0.02	0.49 ± 0.01	0.85 ± 0.00	1.48 ± 0.04	0.86 ± 0.01
Branch stem	0.41 ± 0.01	0.61 ± 0.02	0.45 ± 0.00	0.82 ± 0.01	1.55 ± 0.02	0.91 ± 0.02
Main stem	0.40 ± 0.01	0.54 ± 0.02	0.41 ± 0.01	0.80 ± 0.01	1.62 ± 0.01	0.94 ± 0.01
Root	0.39 ± 0.02	0.55 ± 0.03	0.41 ± 0.01	0.78 ± 0.03	1.59 ± 0.02	0.94 ± 0.03
RSD[a]	0.08	0.26	0.35	0.06	0.12	0.08

[a] Relative standard deviation (RSD), defined as the ratio of standard deviation to mean value for each column

of two bands at 1 050 cm^{-1} ($I_{1\,050}$) and 895 cm^{-1} (I_{895}) decrease in general from root material, to main stem, branch stem, petiole, and leaf blade specimen, while the reproductive material increases in the two intensities compared with the leaf blade sample. The intensity of the 1 730 cm^{-1} ($I_{1\,730}$) band increases from root samples, to main stem, branch stem, and petiole, and then decreases from petiole to leaf blade and increases from leaf blade to reproductive sample. This is expected, as the three bands at 1 620, 1 525, and 1 235 cm^{-1} are related to protein and amine compositions and other bands at 1 730, 1 050, and

895 cm^{-1} are due to carbohydrate derivatives. Relative standard deviation (RSD), calculated from the ratio of standard deviation (SD) to mean value, shows the variation of six biomasses for a specific IR intensity index. In general, the $I_{1\,525}$ value possesses the greatest RSD of 0.35, followed by the $I_{1\,620}$ index (RSD = 0.26), the $I_{1\,050}$ index (RSD = 0.12), the $I_{1\,730}$ and I_{895} values (RSD = 0.08), as well as the $I_{1\,235}$ values (RSD = 0.06). Hence, changes in intensities of six FT-IR indices reveal differing biosynthesis mechanisms of Amide/amine and C–C/C–O
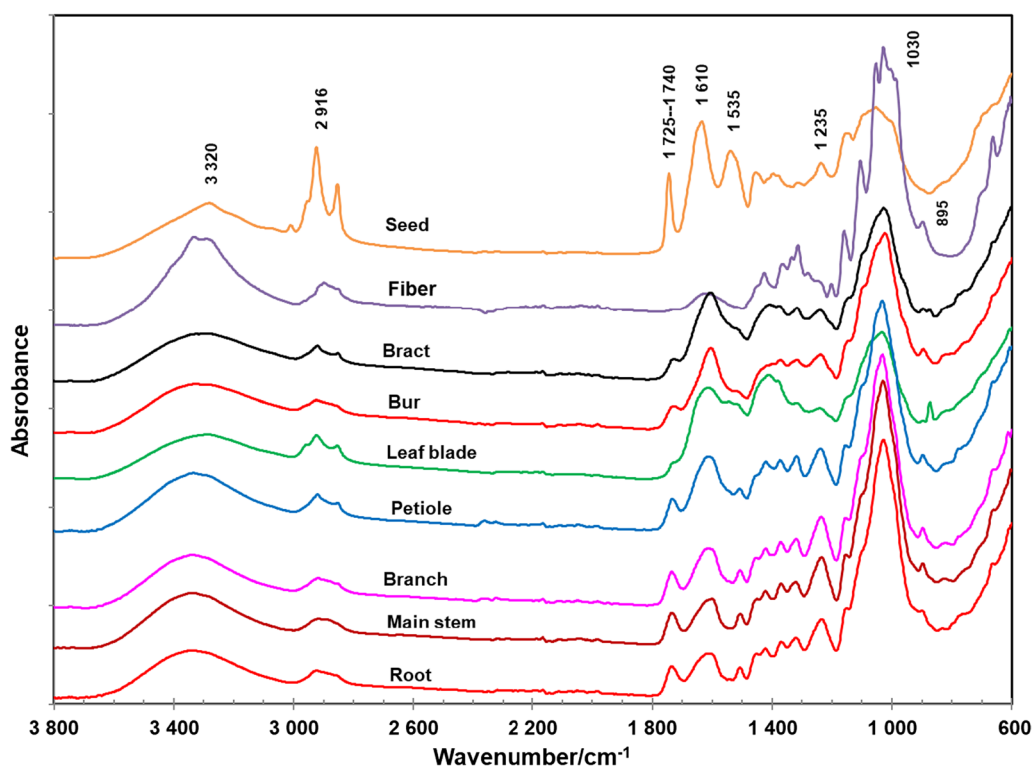
Fig. 5 ATR FT-IR spectra of nine different cotton organs and tissues collected from cotton plants at the maturation stage

functional groups between these cotton plant parts, respectively.

ATR FT-IR features of nine biomass samples collected at the maturation stage

Unique and characteristic FT-IR bands for individual cotton plant parts in Fig. 5 represent striking and reasonable differences of biomass origins during the fiber maturation stage. Cotton fibers and seeds are two extreme portions, and their spectral features differ from those of other cotton plant parts significantly. Commonly, cellulose is a major chemical component in mature cotton fibers (Hsieh 2007), while oils, proteins, fats, highly digestible fibers, and inorganic minerals are abundant in cotton seeds (He and Liu 2021; Rohman and Man 2010; Talpur et al. 2014). Obvious FT-IR spectral difference between cotton fiber and other cotton plant portions is the absence of two unique bands at 1 725 and 1 235 cm^{-1} in cotton fiber, which come from the C=O groups in carboxylic acids of cellulosic derivatives and N–H deformation modes in proteins, respectively. Characteristic FT-IR bands of cotton seeds are two strong and separated absorption bands at 1 745 and 1 535 cm^{-1} from the respective ester C=O group and Amide II mode in two major components of cotton seeds (i.e., oil and protein). Compared with the spectra of both cotton fiber and seed, FT-IR spectra of some cotton plant biomass have been investigated before (Himmelsbach et al. 2006), primarily because these cotton plant parts are the undesired contaminants (or foreign matters) mingled into commercial cotton bales. There were expected chemical, compositional, and structural differences of plant biomass between reproductive stage and maturation stage, as revealed by principal component analysis (PCA) of their FT-IR spectra (Liu et al. 2016). The results showed a tendency of the first principal component (PC1) scores increasing with plant samples in the order of main stems < root = branches < petioles < burs < reproductive = bracts < leaf blades, and also of the second principal component (PC2) score separating the same type of plant parts collected at reproductive stage and maturation stage.

Similar to the pattern in Table 1, Table 2 shows the intensity for the two bands at 1 620 cm^{-1} ($I_{1\,620}$) and 1 525 cm^{-1} ($I_{1\,525}$) increasing initially from root sample to main stem, branch stem, petiole and leaf blade, then the intensity of these two bands decreasing from leaf blade to burr and bract samples at the maturation stage. It also indicates the intensity for the two bands at 1 050 cm^{-1} (I_{1050}) and 895 cm^{-1} (I_{895}) decreasing from root to main stem, branch stem, petiole, and leaf blade, and the intensity increasing from leaf blade to bur and bract substance. Because of the fact that fibers consist of cellulose component dominantly, while cotton seeds include oils and proteins as major compositions, it is anticipated a distinctive pattern between the two in Table 2. Compared with the same indices among the nine materials, the fiber sample is with the largest $I_{1\,050}$ and I_{895} indices and also the smallest $I_{1\,730}$, $I_{1\,620}$, $I_{1\,525}$, and $I_{1\,235}$ indices. On the other hand, the seed material has the least I_{895} indices, but the greatest $I_{1\,730}$, $I_{1\,620}$, and $I_{1\,235}$ indices among the nine materials. In addition, RSD of nine biomasses from the maturation stage (Table 2) decreases in the order of the $I_{1\,525}$ value (RSD = 0.36), the $I_{1\,620}$ value (RSD = 0.27), the $I_{1\,730}$ value (RSD = 0.16), the I_{895} value (RSD = 0.14), the $I_{1\,050}$ index (RSD = 0.13), and the $I_{1\,235}$ value (RSD = 0.12). The tendency of RSD in Table 2 differs slightly from that in Table 1, with the $I_{1\,730}$ and I_{895} values overpassing the $I_{1\,050}$ index. Therefore, variations of six FT-IR indices address the different biosynthesis mechanisms of Amide and C–C/C–O functional groups between these cotton plant biomasses at the maturation stage.

Table 2 The normalized intensities of six ATR FT-IR bands of the plant biomass from the fiber maturity stage. Data are present as average ± standard deviation (n = 4)

	$I_{1\,730}$	$I_{1\,620}$	$I_{1\,525}$	$I_{1\,235}$	$I_{1\,050}$	I_{895}
Seed	0.50 ± 0.08	0.98 ± 0.04	0.92 ± 0.05	0.89 ± 0.02	1.22 ± 0.02	0.72 ± 0.02
Fiber	0.30 ± 0.01	0.42 ± 0.01	0.35 ± 0.01	0.57 ± 0.00	1.69 ± 0.01	1.15 ± 0.02
Bract	0.36 ± 0.01	0.82 ± 0.03	0.72 ± 0.04	0.82 ± 0.01	1.29 ± 0.02	0.90 ± 0.02
Bur	0.39 ± 0.02	0.74 ± 0.02	0.58 ± 0.02	0.85 ± 0.02	1.41 ± 0.02	0.97 ± 0.02
Leaf blade	0.33 ± 0.02	0.91 ± 0.02	0.93 ± 0.02	0.86 ± 0.01	1.18 ± 0.01	0.78 ± 0.02
Petiole	0.40 ± 0.03	0.71 ± 0.05	0.56 ± 0.03	0.82 ± 0.02	1.46 ± 0.06	0.89 ± 0.01
Branch stem	0.46 ± 0.02	0.61 ± 0.02	0.48 ± 0.03	0.88 ± 0.02	1.56 ± 0.03	0.93 ± 0.02
Main stem	0.44 ± 0.01	0.52 ± 0.01	0.42 ± 0.01	0.88 ± 0.01	1.63 ± 0.01	0.98 ± 0.01
Root	0.44 ± 0.01	0.53 ± 0.02	0.41 ± 0.02	0.83 ± 0.00	1.63 ± 0.02	1.04 ± 0.03
RSD[a]	0.16	0.27	0.36	0.12	0.13	0.14

[a] Relative standard deviation (RSD), defined as the ratio of standard deviation to mean value for each column

It is noticeable that there are some spectral intensity differences between the reproductive stage (Table 1) and the maturation stage (Table 2). For example, intensities of the bands at 1 730 and 1 235 cm^{-1} increase among root, main stem, and branch stem , whereas that at 1 050 cm^{-1} decreases among root and petiole from the reproductive stage to the maturation stage. While for leaf blade from the reproductive stage to the maturation stage, apparent spectral intensity reduction occurs in the 1 650–1 480 cm^{-1} region due to noncellulosic components, and intensity increase happens at 870 cm^{-1} due to β-D-fructose (Türker-Kaya and Huck 2017). In order to differentiate the same type of cotton plant biomasses picked at the reproductive stage and the maturation stage, Table 3 compares the changes in averaged values of four field replicates for each sample collected at two periods. Root samples show significant difference in biomass composition by four of six IR indices, followed by main stem and petiole sample with three IR indices, and

also branch stem sample and leaf blade sample with two IR indices. This observation is much in line with expectation, as individual cotton plant organ undergoes unique biosynthesis. On the other hand, the $I_{1\,235}$ index is found to be effective in separating all samples (from root to main stem, branch stem, petiole, and leaf blade) at the maturation stage from those at the reproductive stage, then the $I_{1\,730}$ and I_{895} value, and next the $I_{1\,620}$, $I_{1\,525}$, and $I_{1\,050}$ index.

Chemical composition of cotton fiber

Table 4 lists only the selected chemical components of cotton fiber sample as such composition data of other cotton biomass samples (Additional file 1: Table S1) have been reported previously (He et al. 2017, 2020a). The fiber sample, as it was, contained 5.44% of water (moisture), converted to 57.5 g·kg^{-1} on a dry basis, comparable to about 8% reported before (McCall and Jurgens 1951). As a major element in organic materials, carbon

Table 3 Change in average (n = 4) of six IR intensity values of cotton plant organs and tissue between the reproductive stage and the maturation stage and also their difference statistically

	$I_{1\,730}$	$I_{1\,620}$	$I_{1\,525}$	$I_{1\,235}$	$I_{1\,050}$	I_{895}
Leaf blade	− 0.01	− 0.09***	0.02	− 0.06***	0.01	0.02
Petiole	− 0.01	0.04	0.07**	− 0.03**	− 0.02	0.03*
Branch stem	0.05**	0.00	0.03	0.06**	0.01	0.02
Main stem	0.04***	− 0.02	0.01	0.08***	0.01	0.04**
Root	0.05**	− 0.02	0.00	0.05**	0.04*	0.10**

Symbol *, ** and *** indicate the coefficient value significant at $P = 0.05$, 0.01 and 0.001, respectively

Table 4 Selected chemical components of cotton fiber collected from the maturation stage. Data are present on the dry basis with average (A) and standard deviation (SD, n = 4)

Major component/ *(g·kg^{-1})*	Moisture	Total C	Cellulose	Hemicellulose	Protein	ADL	ADF
A	57.5	385.5	915.2	23.5	22.1	19.3	934.5
SD	1.0	3.3	15.2	14.2	4.5	10.0	8.5
Macro element/ *(g·kg^{-1})*	P	Ca	K	Mg	Na	S	Ash
A	0.59	0.52	5.22	0.63	0.81	0.58	19.95
SD	0.19	0.07	3.97	0.13	0.10	0.10	2.25
Trace element/ *(mg·kg^{-1})*	Fe	Zn	Cu	Mn	B	Ni	Al
A	12.83	5.04	1.67	3.74	50.78	0.29	8.73
SD	5.58	0.33	0.42	0.11	38.19	0.21	4.42

ADL acid detergent lignin, *ADF* acid detergent fiber

HE *et al. Journal of Cotton Research*   (2022) 5:11

Page 10 of 13

accounted for > 1/3 of the biomass of the cotton fiber sample. It appeared mainly in the form of cellulose, with minor forms of hemicellulose, lignin, protein, and other unmeasured components (e.g., wax, small organic acid) (Wakelyn et al. 2007). The main form was acid detergent fiber (ADF, 934.5 g·kg^{-1}). The difference between ADF and acid detergent lignin (ADL, 19.3 g·kg^{-1}) was the content of cellulose (915.2 g·kg^{-1}) of the tested fiber sample. This cellulose value was quite consistent with the historic data of the cellulose content ranging from 880 to 960 g·kg^{-1} (McCall and Jurgens 1951). Combined our result with other cellulose measurements in last couple of decades (Corradini et al. 2009; de Morais Teixeira et al. 2010), methodology evolution from that one in 1950's (McCall and Jurgens 1951) has not greatly impacted the measurement of fiber cellulose much. In contrast to the cellulose content, contents of protein (22.1 g·kg^{-1}) and ash (19.95 g·kg^{-1}) in our fiber sample were higher than the historic ranges of 11~19 g·kg^{-1} and 7~16 g·kg^{-1}, respectively (McCall and Jurgens 1951; Wakelyn et al. 2007). Our data indicated that the hemicellulose contents in the sample were at the same level of protein and ash around 20 g·kg^{-1}. These values were higher than the content of hemicellulose (5 g·kg^{-1}) in white cotton fiber reported by de Morais Teixeira et al. (2010), but lower than the corresponding value (80.0 g·kg^{-1}) reported by Corradini et al. (2009).

The ash content represented the inorganic salts (phosphates, carbonates, and oxides) and salts of organic acids present in the raw fiber (Wakelyn et al. 2007). Thus, the specific contents of six macro and seven trace elements (minerals) in the fiber samples were measured (Table 4). Those minerals in intact raw cotton enhance fiber's resistance to heat and flame functionally (Nam et al. 2014). As reported by Wakelyn et al. (2007), K was the most abundant macro element (about tenfold higher than other macro elements) in the fiber. While these elements are biologically necessary for the development of the cotton plant and fiber (Tewolde et al. 2018; Wakelyn et al. 2007), uptake of K under Ca-deficient conditions is favorable to

the fiber elongation and maturation (Gamble 2009; Guo et al. 2017). It seems that a high level of Ca results in the formation of rigid fiber morphology to inhibit the fiber elongation (He et al. 2021b). Future investigation of the Ca uptake and distribution from cotton roots to the leaf blade and reproductive organs over the fiber development phase would be helpful to investigate if higher Ca expression activity or Ca signaling genes are involved in the inhibitory mechanisms of fiber elongation.

Correlation analysis of the ATR FT-IR parameters and chemical composition measurements

Correlation analysis is useful to elucidate the relationships between chemophysical properties and FT-IR features in agricultural studies (He et al. 2017, 2021a; Waldrip et al. 2014). Thus, the correlation coefficients of the six major chemical composition measurements (i.e., the content of cellulose, hemicellulose, protein, ADL, ADF, and ash) and the six fingerprinting FT-IR bands with all biomass samples collected at both the reproductive stage and the maturation stage were calculated (Table 5). There were 13 of 36 pairs of data between the two measurements showing the correlation coefficients significant at $P \leq 0.05$. The FT-IR intensities of $I_{1\,620}$ and $I_{1\,525}$ are only positively correlated to the protein content, indicating that the two FT-IR bands could be used to monitor the protein synthesis and abundance during the cotton growth. Previously, Waldrip et al. (2014) reported that the FT-IR intensity at 1 650 cm^{-1} was positively correlated ($P \leq 0.05$) to N forms in cattle manure samples. Similarly, the increase of $I_{1\,235}$ is correlated exclusively to the increase of cellulose content. The intensity of $I_{1\,050}$ was an indicator of hemicellulose content apparently. On the other hand, the change of I_{895} is positively correlated to cellulose, hemicellulose, and ADF contents, indicating I_{895} as a general carbohydrate parameter, but not serving well as an exclusive measurement to any of the three. As a comparison, two separate studies reported strong and linear relationships between the integrated intensity

Table 5 Correlation coefficients between the six ATR FT-IR indices and six chemical properties of all plant biomass samples collected at both the reproductive stage and the maturation stage (n = 15)

	$I_{1\,730}$	$I_{1\,620}$	$I_{1\,525}$	$I_{1\,235}$	$I_{1\,050}$	I_{895}
Cellulose	− 0.475	− 0.464	− 0.352	0.894***	0.403	0.644*
Hemicellulose	0.260	− 0.753*	− 0.672*	− 0.653*	0.784**	0.685*
Protein	− 0.408	0.657*	0.726*	− 0.030	− 0.684*	− 0.469
ADL	− 0.423	0.032	0.131	− 0.329	− 0.101	0.302
ADF	− 0.478	− 0.460	0.347	− 0.894***	0.398	0.644*
Ash	− 0.768**	0.194	0.313	− 0.483	− 0.311	0.062

Symbol *, ** and *** indicate the coefficient value significant at $P = 0.05$, 0.01, and 0.001, respectively

HE *et al. Journal of Cotton Research*   (2022) 5:11

Page 11 of 13

of the 895 cm^{-1} band and cellulose content in developmental cotton fibers (Abidi et al. 2014; Liu and Kim 2017). Those statistically significantly negative correlation coefficients are the indicators of the competitively reversing change trends of the functional groups assigned to the FT-IR bands with the chemical component measured. For example, the negative correlation between $I_{1\,730}$ and ash content suggests that the change of minerals (ash) content was in a reverse order with the organic acid level ($I_{1\,730}$) in these cotton tissues. This observation may imply that most minerals (if not all) in these cotton plant materials do not form biominerals (such as Ca oxalate) as reported in some species of Cacteae grown under desert environment (la Rosa-Tilapa et al. 2020). No statistically significant correlation between ADL and any FT-IR bands implied that rapid FT-IR evaluation was not very useful for ADL estimates from the current ADL testing procedure. Although two FT-IR bands are significantly correlated to ADF, application of the whole spectral range with a regression method of modified minimum partial least squares could be an alternative in ADF quantification, as in an analysis of ADF of turnip greens and tops (Obregón-Cano et al. 2019).

Conclusions

ATR FT-IR spectroscopy in combination with statistical analysis was applied to evaluate a series of cotton plant tissues (biomass parts), including the root, stems, leaves, and reproductive parts, at reproductive and maturation stages. The FT-IR spectra displayed distinct spectral patterns, especially in the lower wavenumber range with recognizable functional group characteristics of the biomass parts studied. Correlation coefficient analysis of the six FT-IR bands in the fingerprinting region with six major chemical components revealed that the FT-IR band intensities at 1 620, 1 525, 1 235, and 1 050 cm^{-1} were exclusively and positively correlated to the levels of protein (amide I), protein (amide II), cellulose, and hemicellulose of the 15 cotton biomass samples tested, respectively, at $P \leq 0.05$. The negative correlations ($P \leq 0.05$) between the organic acid-related $I_{1\,730}$ and ash content implied that the presence of minerals and small organic acid molecules was in a complementary mode in these cotton tissues. These resulting observations of ATR FT-IR analysis were sufficiently unique to be used as fingerprinting to monitor the synthesis, transport, accumulation, and other biological implications of these major chemical components in various cotton tissues over the cotton growth period.

Supplementary Information

Declarations

Author details
[1]Southern Regional Research Center, USDA-ARS, New Orleans, LA 70124, USA. [2]Crop Science Research Laboratory, USDA-ARS, Mississippi State, MS 39762, USA. [3]Department of Plant and Soil Sciences, Oklahoma State University, Stillwater, OK 74078, USA.

References
Abidi N, Manike M. X-ray diffraction and FTIR investigations of cellulose deposition during cotton fiber development. Text Res J. 2018;88:719–30.

Abidi N, Cabrales L, Haigler CH. Changes in the cell wall and cellulose content of developing cotton fibers investigated by FTIR spectroscopy. Carbohydr Polym. 2014;100:9–16.

Al Afif R, Anayah SS, Pfeifer C. Batch pyrolysis of cotton stalks for evaluation of biochar energy potential. Renew Energy. 2020;147:2250–8. https://doi.org/10.1016/j.renene.2019.09.146.

Allen A, Foulk J, Gamble G. Preliminary Fourier-transform infrared spectroscopy analysis of cotton trash. J Cotton Sci. 2007;11:68–74.

Bekiaris G, Bruun S, Peltre C, et al. FTIR–PAS: a powerful tool for characterising the chemical composition and predicting the labile C fraction of various organic waste products. Waste Manag. 2015;39:45–56. https://doi.org/10.1016/j.wasman.2015.02.029.

Bekiaris G, Peltre C, Barsberg ST, et al. Comparison of three different FTIR sampling techniques (diffuse reflectance, photoacoustic and attenuated total

HE *et al. Journal of Cotton Research*   (2022) 5:11

Page 12 of 13

reflectance) for the characterisation of bio-organic samples. J Environ Qual. 2020;49:1310–21. https://doi.org/10.1002/jeq2.20106.

Bellaloui N, Turley R, Stetina S, et al. Cottons eed protein, oil, and mineral nutrition in near-isogenic *Gossypium hirsutum* cotton lines expressing leaf color phenotypes under field conditions. Food Nutri Sci. 2019;10:834–59. https://doi.org/10.4236/fns.2019.107061.

Bellaloui N, Turley RB, Stetina SR. Cottonseed protein, oil, and minerals in cotton (*Gossypium hirsutum* L.) lines differing in curly leaf morphology. Plants. 2021;10:525. https://doi.org/10.3390/plants10030525.

Brown DM, Zeef LA, Ellis J, et al. Identification of novel genes in *Arabidopsis* involved in secondary cell wall formation using expression profiling and reverse genetics. Plant Cell. 2005;17:2281–95.

Cheng HN, Kilgore K, Ford C, et al. Cottonseed protein-based wood adhesive reinforced with nanocellulose. J Adhes Sci Technol. 2019;33:1357–68. https://doi.org/10.1080/01694243.2019.1596650.

Cheng HN, He Z, Ford C, et al. A review of cottonseed protein chemistry and non-food applications. Sustain Chem. 2020;1:256–74. https://doi.org/10.3390/suschem1030017.

Corradini E, Teixeira E, Paladin P, et al. Thermal stability and degradation kinetic study of white and colored cotton fibers by thermogravimetric analysis. J Therm Anal Calorim. 2009;97:415–9.

de Morais TE, Corrêa AC, Manzoli A, et al. Cellulose nanofibers from white and naturally colored cotton fibers. Cellulose. 2010;17:595–606.

Egbuta M, McIntosh S, Waters D, et al. Biological importance of cotton by-products relative to chemical constituents of the cotton plant. Molecules. 2017;22(1):93. https://doi.org/10.3390/molecules22010093.

Fortier CA, Rodgers JE, Cintron MS, et al. Identification of cotton and cotton trash components by Fourier transform near-infrared spectroscopy. Text Res J. 2011;81:230–8.

Fortier CA, Santiago CM, Rodgers JE, et al. Fourier-transform imaging of cotton and botanical and field trash mixtures. Fibers. 2017;5:1–11.

Gamble GR. Regional, varietal, and crop year variations of metal contents associated with the separate structural components of upland cotton (*Gossypium hirsutum*) fiber. J Cotton Sci. 2009;13:221–6.

Goydaragh MG, Taghizadeh-Mehrjardi R, Jafarzadeh AA, et al. Using environmental variables and Fourier transform infrared spectroscopy to predict soil organic carbon. CATENA. 2021;202: 105280. https://doi.org/10.1016/j.catena.2021.105280.

Guo K, Tu L, He Y, et al. Interaction between calcium and potassium modulates elongation rate in cotton fiber cells. J Exp Bot. 2017;68:5161–75. https://doi.org/10.1093/jxb/erx346.

He Z, Liu Y. Fourier transform infrared spectroscopic analysis in applied cotton fiber and cottonseed research: a review. J Cotton Sci. 2021;25:167–83.

He Z, Ohno T, Cade-Menun BJ, et al. Spectral and chemical characterization of phosphates associated with humic substances. Soil Sci Soc Am J. 2006;70:1741–51.

He Z, Mao J, Honeycutt CW, et al. Characterization of plant-derived water extractable organic matter by multiple spectroscopic techniques. Biol Fertil Soils. 2009;45:609–16.

He Z, Honeycutt CW, Zhang H. Elemental and Fourier transform infrared spectroscopic analysis of water and pyrophosphate extracted soil organic matter. Soil Sci. 2011;176:183–9. https://doi.org/10.1097/SS.0b013e318212865c.

He Z, Zhang H, Olk DC, et al. Protein and fiber profiles of cottonseed from upland cotton with different fertilizations. Mod Appl Sci. 2014;8(4):97–105. https://doi.org/10.5539/mas.v8n4p97.

He Z, Uchimiya SM, Guo M. Production and characterization of biochar from agricultural by-products: overview and use of cotton biomass residues. In: Guo M, He Z, Uchimiya SM, editors. Agricultural and environmental applications of biochar: advances and barriers. SSSA special publication 63. Madison, WI, USA: Soil Science Society of America, Inc.; 2016. p. 63–86. https://doi.org/10.2136/sssaspecpub63.2014.0037.5.

He Z, Zhang H, Tewolde H, et al. Chemical characterization of cotton plant parts for multiple uses. Agric Environ Lett. 2017;2:110044. https://doi.org/10.2134/ael2016.11.0044.

He Z, Olk DC, Tewolde H, et al. Carbohydrate and amino acid profiles of cotton plant biomass products. Agriculture. 2020a;10:2. https://doi.org/10.3390/agriculture10010002.

He Z, Zhang D, Olanya OM. Antioxidant activities of the water-soluble fractions of glandless and glanded cottonseed protein. Food Chem. 2020b;325: 126907. https://doi.org/10.1016/j.foodchem.2020.126907.

He Z, Zhang H, Fang DD, et al. Effects of inter-species chromosome substitution on cottonseed mineral and protein nutrition profiles. Agron J. 2020c;112:3963–74. https://doi.org/10.1002/agj2.20264.

He Z, Guo M, Fortier C, et al. Fourier transform infrared and solid state ^{13}C nuclear magnetic resonance spectroscopic characterization of defatted cottonseed meal-based biochars. Mod Appl Sci. 2021a;15(1):108–21. https://doi.org/10.5539/mas.v15n1p108.

He Z, Nam S, Fang DD, et al. Surface and thermal characterization of cotton fibers of phenotypes differing in fiber length. Polymers. 2021b;13:994. https://doi.org/10.3390/polym13070994.

Himmelsbach DS, Akin DE, Kim J, et al. Chemical structural investigation of the cotton fiber base and associated seed coat: Fourier-transform infrared mapping and histochemistry. Text Res J. 2003;73:281–8.

Himmelsbach DS, Hellgeth JW, McAlister DD. Development and use of an attenuated total reflectance/Fourier transform infrared (ATR/FT-IR) spectral database to identify foreign matter in cotton. J Agric Food Chem. 2006;54:7405–12.

Hsieh YL. Chemical structure and properties of cotton. In: Gordon S, Hsieh YL, editors. Cotton: science and technology. Cambridge, UK: Woodhead Publishing Limited; 2007.

Hssaini L, Elfazazi K, Razouk R, et al. Combined effect of cultivar and peel chromaticity on figs' primary and secondary metabolites: preliminary study using biochemical and FTIR fingerprinting coupled to chemometrics. Biology. 2021;10:573. https://doi.org/10.3390/biology10070573.

Kim HJ. Fiber biology. In: Fang DD, Percy RG, editors. Cotton. 2nd ed. Madison, WI, USA: American Society of Agronomy, Crop Science Society of America, Soil Science Society; 2015. p. 97–127.

Kim HJ, Lee CM, Dazen K, et al. Comparative physical and chemical analyses of cotton fibers from two near isogenic upland lines differing in fiber wall thickness. Cellulose. 2017;24:2385–401. https://doi.org/10.1007/s10570-017-1282-1.

Kirkan B, Sarikurkcu C, Copuroglu M, et al. Is it possible to use the stalks of *Gossypium hirsitum* L., an important by-product of cotton cultivation, as an alternative source of bioactive components? Eur Food Res Technol. 2018;244:1065–71. https://doi.org/10.1007/s00217-017-3029-5.

Kumar M, Tomar M, Punia S, et al. Cottonseed: a sustainable contributor to global protein requirements. Trends Food Sci Technol. 2021;111:100–13. https://doi.org/10.1016/j.tifs.2021.02.058.

Kurtulbaş E, Bilgin M, Şahin S. Assessment of lipid oxidation in cottonseed oil treated with phytonutrients: kinetic and thermodynamic studies. Ind Crops Prod. 2018;124:593–9. https://doi.org/10.1016/j.indcrop.2018.08.039.

la Rosa-Tilapa D, Maceda A, Terrazas T. Characterization of biominerals in Cacteae species by FTIR. Curr Comput-Aided Drug Des. 2020;10:432. https://doi.org/10.3390/cryst10060432.

Lazzari E, Schena T, Marcelo MCA, et al. Classification of biomass through their pyrolytic bio-oil composition using FTIR and PCA analysis. Ind Crop Prod. 2018;111:856–64. https://doi.org/10.1016/j.indcrop.2017.11.005.

Liu Y, Kim HJ. Fourier transform infrared spectroscopy (FT-IR) and simple algorithm analysis for rapid and non-destructive assessment of developmental cotton fibers. Sensors. 2017;17:469. https://doi.org/10.3390/s17071469.

Liu Y, Thibodeaux D, Gamble G. Development of Fourier transform infrared spectroscopy in direct, non-destructive, and rapid determination of cotton fiber maturity. Text Res J. 2011;81:1559–67. https://doi.org/10.1177/0040517511410107.

Liu Y, Thibodeaux D, Gamble G. Characterization of attenuated total reflection infrared spectral intensity variations of immature and mature cotton fibers by two-dimensional correlation analysis. Appl Spectrosc. 2012;66:198–207. https://doi.org/10.1366/11-06440.

Liu Y, He Z, Uchimiya M. Comparison of biochar formation from various agricultural by-products using FTIR spectroscopy. Mod Appl Sci. 2015;9(4):246–53. https://doi.org/10.5539/mas.v9n4p246.

Liu Y, He Z, Shankle M, Tewolde H. Compositional features of cotton plant biomass fractions characterized by attenuated total reflection Fourier transform infrared spectroscopy. Ind Crop Prod. 2016;79:283–6. https://doi.org/10.1016/j.indcrop.2015.11.022.

HE *et al. Journal of Cotton Research*   *(2022) 5:11*

Page 13 of 13

Liyanage S, Abidi N. Molecular weight and organization of cellulose at different stages of cotton fiber development. Text Res J. 2019;89:726–38. https://doi.org/10.1177/0040517517753642.

McCall ER, Jurgens JF. Chemical composition of cotton. Text Res J. 1951;21:19–21.

Mollaee M, Mobli A, Kaur NK, et al. Challenges and opportunities in cotton production. In: Jabran K, Chauhan BS, editors. Cotton production. New York, USA: Wiley; 2020. p. 371.

Nam S, Condon BD, Foston MB, et al. Enhanced thermal and combustion resistance of cotton linked to natural inorganic salt components. Cellulose. 2014;21:791–802. https://doi.org/10.1007/s10570-013-0133-y.

Nam S, Condon BD, Liu Y, He Q. Natural resistance of raw cotton fiber to heat evidenced by the suppressed depolymerization of cellulose. Polym Degrad Stab. 2017;138:133–41. https://doi.org/10.1016/j.polymdegradstab.2017.03.005.

Natalio F, Maria R. Structural evolution of *Gossypium hirsutum* fibers grown under greenhouse and hydroponic conditions. Fibers. 2018;6:11.

Obregón-Cano S, Moreno-Rojas R, Jurado-Millán AM, et al. Analysis of the acid detergent fibre content in turnip greens and turnip tops (*Brassica rapa* L. Subsp. rapa) by means of near-infrared reflectance. Foods. 2019;8:364. https://doi.org/10.3390/foods8090364.

Oosterhuis DM, Jernstedt J. Morphology and anatomy of the cotton plant. In: Smith CW, Cothren JT, editors. Cotton: origin, history, technology, and production. New York, USA: Wiley; 1999. p. 175–206.

Renuka CK, Kumarmath PS, Kadakol JC, et al. Chemical composition and antinutritional factors in different parts and whole cotton (*Gossypium hirsutum*) plant. Karnataka J Agric Sci. 2005;18:114–7.

Robertson WC, Roberts BA. Integrated crop management for cotton production in the 21st century. In: Wakelyn PJ, Chaudhry MR, editors. Cotton technology for the 21st century. Washington, DC, USA: International Cotton Advisory Committee; 2010. p. 63–9.

Rohman A, Man YBC. Fourier transform infrared (FTIR) spectroscopy for analysis of extra virgin olive oil adulterated with palm oil. Food Res Int. 2010;43:886–92.

Shakhidoyatov KM, Rashkes A, Khidyrova N. Components of cottonplant leaves, their functional role and biological activity. Chem Nat Compd. 1997;33:605–16.

Talpur MY, Kara H, Sherazi STH, et al. Application of multivariate chemometric techniques for simultaneous determination of five parameters of cottonseed oil by single bounce attenuated total reflectance Fourier transform infrared spectroscopy. Talanta. 2014;129:473–80.

Tewolde H, Shankle MW, Way TR, et al. Enhancing management of fall-applied poultry litter with cover crop and subsurface band placement in no-till cotton. Agron J. 2015;107:449–58. https://doi.org/10.2134/agronj14.0266.

Tewolde H, Shankle MW, Way TR, et al. Poultry litter band placement affects accessibility and conservation of nutrients and cotton yield. Agron J. 2018;110:675–84. https://doi.org/10.2134/agronj2017.07.0387.

Türker-Kaya S, Huck CW. A review of mid-infrared and near-infrared imaging: principles, concepts and applications in plant tissue analysis. Molecules. 2017;22:168. https://doi.org/10.3390/molecules22010168.

Vancov T, Palmer J, Keen B. A two stage pretreatment process to maximise recovery of sugars from cotton gin trash. Bioresour Technol Rep. 2018;4:114–22. https://doi.org/10.1016/j.biteb.2018.09.010.

Wakelyn PJ, Bertoniere NR, French AD, et al. Cotton fiber chemistry and technology. Boca Raton, FL, USA: CRC Press; 2007.

Waldrip HM, He Z, Todd RW, et al. Characterization of organic matter in beef feedyard manure by ultraviolet-visible and Fourier transform infrared spectroscopies. J Environ Qual. 2014;43:690–700. https://doi.org/10.2134/jeq2013.09.0358.

Yue H, Zheng Y, Zheng P, et al. On the improvement of properties of bioplastic composites derived from wasted cottonseed protein by rational cross-linking and natural fiber reinforcement. Green Chem. 2020;22:8642–55. https://doi.org/10.1039/D0GC03245J.

Zhang L, Li X, Zhang S, et al. Micro-FTIR combined with curve fitting method to study cellulose crystallinity of developing cotton fibers. Anal Bioanal Chem. 2021;413:1313–20. https://doi.org/10.1007/s00216-020-03094-6.